

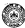
A STUDY ON TOOL LIFE OF GRINDING WHEELS

By

JAGDISH PRASAD MEHTA

Mr. (M.Tech.)
B.Tech.

Q



DEPARTMENT OF MECHANICAL ENGINEERING
INDIAN INSTITUTE OF TECHNOLOGY KARUR
TAMIL NADU

A STUDY ON TOOL LIFE OF GRINDING WHEELS

A Thesis submitted
In Partial Fulfilment of the Requirements
for the Degree of
MASTER OF TECHNOLOGY

By
JAGDISH PRASAD MEHTA

1988

DEPARTMENT OF MINERALS ENGINEERING
INDIAN INSTITUTE OF TECHNOLOGY KANPUR
AUGUST 1988



I.I.T. KANPUR
CENTRAL LIBRARY

Acc. No. **A 28878**

26 AUG 1978

ME-1734-M-MLH-STU

TH-

MR. LEE DREW M.

RECORDED

Certified that this work on "A Study of the Use of GEL/PMMA
GELS" by Jagdish Prasad Nalde has been carried out under my supervision
and that this work has not been submitted elsewhere for a degree.


Dr. D. S. Lal
Associate Professor
Department of Mechanical Engineering
Indian Institute of Technology, Kharagpur

9. 9. 74 24

ACKNOWLEDGEMENT

I am deeply indebted to Mr. G.S. Lal for his invaluable counsel, encouragement, guidance and the confidence he has inspired in me to make this work possible in the present form.

I wish to express my sincere appreciation of the assistance I obtained from Mr. Jaginder Singh, Senior Technical Assistant in the Department of Mechanical Engineering.

I remain grateful to my friends especially Mr. G.B. Bajaj and Mr. R. Mehta for many valuable and fruitful discussions with them.

I wish to thank Mr. R.P. Mehta for typing the manuscript neatly.

J.P. Mehta.

		(yr)
		<u>CONTINUATION</u>
		Page (xx)
CHAPTER 1		INTRODUCTION & SYSTEMATIC ANALYSIS
1.1	General	3
1.2	Structural Risk Analysis of an Individual Frame	3
1.3	Code Thickness	4
1.4	Structuring Action	4
1.5	Opposing Thrusts	5
	1.5.1 Types of Thrusts	5
	1.5.2 Typical Thrust Pattern	7
1.6	Present Work	8
CHAPTER 2		THREE-DIMENSIONAL DESIGNER
2.1	General	12
2.2	Design Requirements	12
2.3	Power Measuring Devices	13
2.4	The Structures Bridge	13
2.5	Bridge Rings	14
2.6	Bridge Equations	15
	2.6.1 Marine Ring Thickness	15
	2.6.2 Vertical Frequency of the Ring	15
2.7	Bridge Calculations	16
	2.7.1 Material Selection	16

	(v)
	Date:
1.1.1.1	16
1.1.1.2	17
1.1.2	18
1.2	19
1.3	20
CHAPTER 2	
EXPERIMENTAL DESIGN	
2.1	21
2.2	22
2.3	23
2.4	24
2.5	25
CHAPTER 3	
RESULTS AND DISCUSSION	
3.1	26
3.2	27
3.3	28
3.4	29
3.5	30
3.6	31
3.7	32
3.8	33
CHAPTER 4	
DISCUSSION	
4.1	34
4.2	35
4.3	36
4.4	37
4.5	38
4.6	39
4.7	40
4.8	41
4.8.1	42
4.8.2	43
4.9	44
4.10	45

		(iv)
		Index
CHAPTER 1.		
1.1.	Classification	11
1.2.	Properties	12
1.3.	Practical Application of the Present Work	13
1.4.	Scope for Further Work	14
REFERENCES		15

DEFINITIONS

- a
 - Number of active arms in the sheathless bridge
- b
 - Mean width of ship
- b_T
 - Width of the ring/rectangle
- b_w
 - Width of the webplane
- c
 - Static constant of tool life equation
- c_1
 - Number of cutting edges per unit area of sheet face
- c_2
 - Equivalent diameter
- c_3
 - Mean diameter
- c_4
 - Reduction in sheet diameter
- c_5
 - Back diameter
- c_6
 - Depth of cut
- c_7
 - Young's modulus of dynamometer ring material
- c_8
 - Input voltage to sheathless bridge
- c_9
 - Normal force component
- c_{10}
 - Tangential force component
- c_{11}
 - Natural frequency of dynamometer ring
- c_{12}
 - Stripping ratio
- c_{13}
 - Gauge factor of strain gauge
- c_{14}
 - Height of the webplane
- $c_{15}, c_{16}, c_{17}, c_{18}$
 - Constants of calibration curve
- l
 - Length of ship
- l_w
 - Length of webplane
- l_T
 - Length of the dynamometer ring

σ_{tensile}	• Yield limit of cylinder when the force of cylinder is equal to zero
σ_{y}	• Response of test life equation
σ_{p}	• Resistance of strain gauge
σ_{c}	• Ratio of mean width to mean thickness of strip
σ_{g}	• Change in resistance of the strain gauge
σ_{t}	• Radius of tensile surface of the orthogonal ring
σ_{r}	• Deflection due to normal force
σ_{g}	• Deflection due to tangential force
σ_{f}	• Spring constant of the diametral ring
σ_{p}	• Rock life of printing sheet in seconds
σ_{t}	• Maximum gauge thickness
σ_{p}	• Minimum thickness of the orthogonal ring
σ_{r}	• Wheel speed
σ_{t}	• Table speed
σ_{g}	• Material removal rate
σ_{g}	• Volume of material removed
σ_{g}	• Longitudinal tensile strain in the strain gauge
σ_{max}	• Maximum stress induced in the orthogonal ring

RESULTS

Tool life of grinding wheels may be established from the consideration of grinding forces, wheel wear and surface finish. In the present work experimental study of horizontal surface grinding process has been carried out to investigate force relations using a transversal dynamometer which can determine the tool forces. From these plots tool life of grinding wheel has been evaluated and an attempt has been made to establish the possible existence of an empirical relationship for tool life under various cutting conditions. The tool life has been found to be function of ratio of peripheral speed, $\frac{V}{n}$. Although quantitatively it is, however, interested since the data available were limited.

Reduction in wheel diameter has been measured to find the influence of wheel wear from which economic considerations for the selection of grinding wheels has been investigated. Experiments also show that an optimum grinding wheel is obtained when various grinding wheels are used for a particular material. This should be an important consideration in the selection of grinding wheels.

CHAPTER-1

INTRODUCTION AND LITERATURE REVIEW

1.1 General

In any ball-milling process a host of basic geometry and concentration is used, but in grinding a large number of grains, acting as cutting points are randomly distributed across the surface of the wheel. High cutting speed (about 2000 rpm), small grain depth of cut (about 10 μm per load) and considerable size (the per to small lateral extent of an individual grain), are the three aspects in which grinding differs from single point cutting. The geometry of abrasive grains not only causes from grain to grain but it also changes continuously as the grinding is continued. Thus, in grinding, the efficiency variable of ball-milling such as wear angles etc., which are as important in the theoretical study and not be measured directly, but instead only a average can be taken of all grains involved in the process.

The specific energy (energy required to remove a unit volume of material) in grinding has been found to be about 10 times that involved in tensile (11). This has been explained in terms of the "size effect". It is a matter of common experience that the greater the degree of subdivision (involved in disintegrating a body), the greater is the energy expended.

In the grinding operation, the chip are very finely divided so that this form of material removal may be expected to require a high specific energy. It has been found (11) that when the surface chip thickness is less than about 20×10^{-3} in., the shear strength of the metal approaches the theoretical value. The attainment of this theoretical value of strength has been attributed to the grain depth of cut, being so small that the material is sheared between the abrasive grains.

3.2 Effective rake angles of an individual grain

In single point cutting it has been found (12) that the ratio of tangential to normal force is strongly dependent on the rake angle of the tool. This ratio decreases as the rake angle is reduced and for tools having large negative rake angles, the value of force ratio approximates 0.5. If this analogy with single point cutting is correct then the typical abrasive grain would, on the average, have a negative rake angle. In their work Becker and Berghaus (13) compared the ratios of the tangential and normal forces obtained when grinding, with those found when turning, and suggested that the mean effective rake angle of a grinding grain should be nearly $\approx 30^\circ$.

As an alternative treatment, Baker (21,22) suggested that it is more realistic to consider the frictional rubbing forces on the abrasive surface and neglect the cutting forces acting on the rake face. This concept led him to introduce his "rubbing grain" hypothesis, in which he emphasized the importance of a dull grit. He observed that when turning

to very small encounter angle ($0^{\circ} \text{ to } 10^{\circ}$) produced no ships at small depth of cut (less than 0.0004 m.). In this regime the force ratio is small due to the forces acting on the encounter face. In this manner ships experienced the small force ratios observed when grinding. However, as change in force ratio is observed with increasing depth of cut even using tools having large negative rake angles [26]. Therefore, the existence of a small force ratio when grinding may be explained in terms of an average cross section + large negative rake angle.

1.2. Ship thickness

Because ship thickness (t) is the most important geometrical quantity in any grinding operation. All ships are assumed to have the same size, and in order to be sure that all the metal to be removed is approximately the same, the ships are assumed to be of constant width (Figs. 1.1, 1.2, 1.3). Actually grinding ships will be shaped as in Fig. 1.2-3, since the main cross-section is the same as in Fig. 1.1-2.

Assuming that the variation of ship thickness is trapezoidal in shape, ship length is given by,

$$L = \sqrt{\frac{2t^2}{d}} \quad \dots \quad \dots \quad \dots \quad (1.1)$$

where,

L = Unformed ship length

t_p = Max. thickness

d = Max. depth of cut.

Centrifugality consideration for metal removal rate given (33)

$$R = \left(\frac{V_w}{V_{ext}} \cdot \sqrt{Q/V_w} \right)^{1/3} \quad \dots \quad \dots \quad \dots \quad (1.2)$$

where,

V_w = Maximum chip thickness

V_{ext} = Table speed

V = Work speed

Q = Number of cutting edges per unit area of work face

$$V = \frac{\text{Nominal width of chip, } b_1}{\text{Nominal thickness of chip, } t_1/2}$$

D_g = Equivalent diameter, depending upon the type of grinding operation.

$$D_g = \frac{D_w + D_b}{2} \quad \dots \quad \text{For external grinding}$$

$$= \frac{D_w - D_b}{2} \quad \dots \quad \text{For internal grinding}$$

$$= D_w \quad \dots \quad \dots \quad \text{For surface grinding}$$

where,

D_w = Work piece diameter.

1.4 Brinell Test:

In order to study grinding action (35) used controlled force plough grinding, in which grinding wheel was pressed against the work piece with prescribed force instead of prescribed feed rate. The radial feed was proportional to the initial steady removal rates. It should be noted that radial feed rate was small under light load and the work piece is ploughed by the

grains forming groove with small metal particles on the sides of the groove. As the load is increased the feed rate increases and beyond a certain load, metal stock removal occurs, these oscillations stops and produces. At very light load there is little or no stock removal and nibbling occurs.

Li & Shek [11] evaluated nibbling action by using coated grinded to produce a single groove on a tapered specimen. They adopted increasing depth of cut by moving the work piece under the wheel. At the beginning of a cut the value of d was small resulting in the ploughing of material to the sides of the groove. At some point along the tapered workpiece the depth of cut approaches the critical value, which defines the nibbling formation. These results are shown in Fig. (1.c). The instantaneous steps in the workpiece portion of the groove and shows the change from ploughing to cutting. They concluded that a curve similar to that shown in Fig. (1.c) will be obtained if the depth of cut are plotted along the strip length. Thus it is possible that there is transition from ploughing to cutting during every cut.

1.3 Grinding Parameters

1.3.1 Form of stock removal

Grindability describes the relative ease of grinding and the susceptibility to oscillability for single point tool cutting. Grindability is mathematically expressed by grinding ratio (ratio of material removed by unit volume of wheel wear). Criterion for grinding stock oscillation is usually based on the optimum grinding ratio.

The nature of grinding wheel wear has been the subject of extensive investigations in the past. The physical properties of abrasives have been discussed by Rogers (4), and by Thompson and Williams (5) while others (12,20,21) have directed their investigations towards the nature of statistical problems. The methods involved in the process have been studied more recently by several investigators (13, 14,15,16,17,18,19,20).

The rate of grinding steel is both physical and chemical in nature. The relative significance of each of these types on the overall wear depends on the characteristics of the work material and grinding conditions.

Physical wear of steel can be understood from the relationship of the physical properties of the abrasive on the wheel and the work material. Three types of physical wear have been observed. These are illustrated in Fig. (1.2).

Ploughing wear occurs on the nondeformable contact surface (a) and it is generally accepted that plastic flow and chemical reaction (20,21) have significant effect on this phenomena. This results in dulling of the abrasive grains and accounts for the glazed appearance of a grinding wheel. When this type of wear is predominant the grinding ratio is high.

Fracture wear, on the other hand, is due to the removal of abrasive particles from the wheel either by partial fracture of grains (b) or by fracturing of the bond part (c) as shown in Fig. 1.2. Fracture wear results in a low grinding ratio but maintains the cutting ability of the wheel by presenting sharp cutting edges without dressing. This phenomena

is called the self-sharpening, which leads to lower cutting forces and lower power. The analysis of fracture wear has been analysed by Tschöp (16) and Beldjedid *et al.* (17) using theories of nucleation and stochastic processes. Their relationship predict the wear rate in terms of the forces in an average grain, the grinding size, amount of heat in the wheel and average size of a fractured grain. A further experimental investigation of fracture wear has been recently carried out by McRae and Cox (18).

1.5.2. Fracture wear regimes:

The sequence of events for flank wear development in single point cutting tool (Fig. 1.4) is initial breaking (region I) where the sharp cutting edge is quickly broken down and a flake wear (and by crystallisation) then uniform wear rate (region II) and the final gradually increasing wear rate (region III). Curves relating the values of grinding wheel wear to the volume of metal removed has been found (23) to be similar in nature to wear curves for a single point cutting tool. Typical grinding wheel wear curve is shown in Fig. 1.6, which shows three distinct regions:

- Region I: A short period of nonlinear rapid wear - when the wheel first contacts the workpiece there is rapid formation of fine sharp points left from the dressing. Grinding ratio in this region is 100.
- Region II: Longer period of constant and slow wear rate - this is the normal operating region of the wheel wear curve, which characterises good grinding conditions. For particular

operating conditions this region gives highest grinding ratio, which is taken as representative value of grinding ratio for these conditions.

Region III: A region of sharp increase in wear rate this results even when the steel is overruled and stable or excessive vibration develops and steel wear rates due to fracture wear which induces attrition wear. This region characterizes poor grinding conditions and results in low value of grinding ratio.

In grinding process and the abrasive grains make repeated contacts with the workpiece, the sharp edges are worn over protective flat areas on the grain. General increase in flat areas increases the force on the grain until it becomes sufficient to cause fracture of the grain or lead just holding the grain. Thus the large percentage of active grain enables this condition grinding (typical Region III). If the bond parts are too strong or grain is not sufficiently brittle then steel face will appear glazed and reworking is required to restore the cutting ability of the grains. If, however, a sheet of paper grain is used, the nature and proportion of attrition and fracture wear may be such that the steel will tend to be self-sharpening, resulting in extended region II, giving optimum grinding ratio.

1.4. *Impact Test:*

Dynamic aspect of grinding process has been discussed by one of the investigators (33,34,35). During the grinding sheet wear study earlier

Shimamoto (17) and Bremmer, Bolliger and Kuehne (4) concluded that loss of shell is mainly due to diagonal dressing. Galt & Powers (20) studied shell life (foot-life between two successive meetings) of grinding shell, and presented approximate relationship between shell life and depth of cut. They concluded in their work that the method they have adopted for establishing shell life was somewhat erratic. Some patterns during grinding was also evaluated by one of the workers (41, 42) but no attempt was made by him to investigate grinding forms with the consideration of depth of grinding. They concluded that the form pattern during grinding is similar to the shell worn away.

It seems that force pattern can be important criteria to predict the shell life of grinding shell. In the present work an attempt has been made to evaluate shell life from the force pattern and correlate it with table speed and depth of cut.

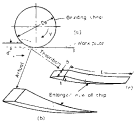


FIG. 1.1 GRINDING GEOMETRY (a)SUBSURFACE GRINDING OPERATION (b) ACTUAL SHAPE OF CHIP (c)THEORETICAL SHAPE OF CHIP



FIG. 1.2 THREE TYPES OF GRINDING WHEEL WEAR

(a) ATTRITIOUS WEAR OF GRAIN

(b) MECHANICAL FRACTURE OF GRAIN

(c) FRACTURE OF BOND BRIDGES

12.5.1.2 EFTS PREDICTION

FIG. 1-5 DETAILED PREDICTION OF PLATE IN AD
WITH TIME

Legend of symbols:

— Current time

— Previous time

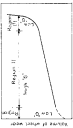
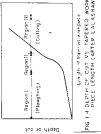
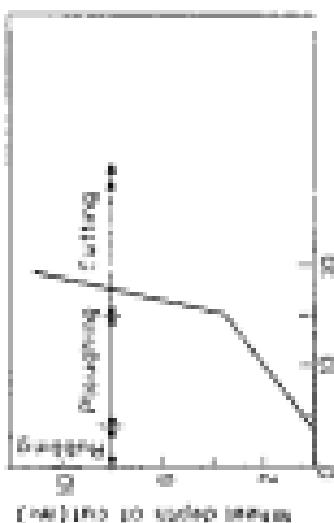


FIG. 1-4 DETAILED PREDICTION OF PLATE IN AD
WITH TIME (CUT-OFF 1 ALARM)

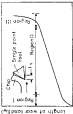


Depth of cut



Mean depth of cut (cm)

FIG. 1-3 EFTS PREDICTION OF PLATE IN AD
WITH TIME



Length of water seal (cm)

CHAPTER 2

MEASUREMENT OF GRINDING FORCES.

2-1. Sensors.

Grinding force is an important parameter in predicting the performance of a grinding wheel. Marshall and Shaw [17] were probably the first to measure grinding forces with the help of a specially designed two-component dynamometer. Since then more sophisticated devices have been built and tested.

2-2. Design Requirements:

The main requirements of a dynamometer which appear each other are sensitivity and stiffness. The sensitivity of a dynamometer should be such that determinations are accurate to within $\pm 1\%$. High stiffness of the dynamometer is also essential to avoid interference with the normal cutting operation of the wheel. In order that the measured force is not influenced by any vibratory action of the dynamometer the natural frequency must be about four times more than that of the exciting vibration [18].

Surface grinding dynamometer should measure the components of the grinding force (that is, axial and tangential components) with adequate cross sensitivity. It should also be stable with respect to time, temperature and humidity.

1.3 Force Measuring Devices

In general force measurement involves the measurement of deflection with a suitable calibration between the force and the deflection it produces. Some devices for measuring such deflections are dial indicators, hydraulic pressure cells, pneumatic devices, piezoelectric crystals and electric resistance strain gauges.

With the development of high quality weighing and recording equipment, heated electric resistance strain gauges are perhaps most suitable for such measuring devices. They can be mounted directly to the transducer ring thus eliminating the need for a separate picking device.

1.4 Sheathless Bridge

Although actual resistance changes in a strain gauge are very small, they are readily measured by connecting the gauges in the form of a sheathless bridge. The gauges are connected in such a way that there is an increase in resistance in opposite arms and decrease in the other two arms, which combine to increase the output voltage. Any equal change in the resistance of adjacent arms gives no output voltage. This property of Sheathless Bridge allows electrical cancellation of unwanted outputs, such as those resulting from temperature changes.

The output voltage from sheathless bridge is given by the following equation (10) :-

$$\Delta V = \frac{R}{4} \frac{\Delta R}{R} \Delta V_0 \quad \text{...1.1} \quad \text{...1.1}$$

where,

a = Number of active arms in the bridge

V_b = Input voltage to the bridge

S_g = Gauge factor of gauge

ϵ = Longitudinal strain in the gauge

Input voltage may be increased to increase the sensitivity of the bridge but heat dissipation capacity of the gauge is the limiting factor in this respect.

3.3 Strain Rings

Strain rings provide a high ratio of sensitivity to stiffness. The fact that the inside surface of the ring is in opposite state of strain from the outside allows true active arm to be advantageously used in a bridge circuit. The greater ⁱⁿ of a ring provides two parallel paths for heat flux which eliminates drift due to temperature gradient in the vicinity of the gauges.

Stress investigation of circular ring shows that points 2,4,7 and 8 (Fig. 3.1) are the strain nodes for normal force F_y and points 1,3,5 and 6 are the strain nodes for tangential force F_x . Also when both components of force are applied, points 1,3,5 and 7 are in tension and others are in compression. Thus by mounting gauges into the uniplanar bridge four components of force can be measured simultaneously with minimum strain sensitivity.

For increasing rigidity we will use truncated octagonal ring instead of a circular one (Figs. 3.1 and 3.2). The gauges will be placed at 45° from vertical axis instead of 30.0°, the theoretical angle. This simplifies

the mounting surface without appreciably affecting the performance. Further if the grooves are symmetrically placed this results in null nonreciprocity.

2.5 Design Equations

2.5.1 Maximum Thickness

In designing dynamo, a compromise must be made between the reliability and the weight. This is controlled mainly by maximum thickness, which is calculated by using following formula, derived from elasticity ring theory (33).

$$t_{\max} = \frac{4 \cdot \delta \cdot F_0 \cdot R_0}{G^2 \cdot b_0 \cdot d_0} \quad \text{mm} \quad \text{mm} \quad \text{mm} \quad (2.2)$$

where,

t_{\max} = Maximum thickness of rectangular ring, mm

F_0 = Normal force, N/mm

G = Young's modulus of ring material, psi

δ = Tensile strain in strain gauges 1 or 2, in/in

b_0 = Width of rectangular ring, mm

d_0 = Radius of the inside surface of ring, mm

2.5.2 Natural Frequency of the Ring

For the purpose of analysis any dynamo can be reduced to a spring supported mass. The natural frequency of such a system is given by,

$$f_n = \frac{1}{2\pi} \sqrt{\frac{F_0}{m}} \quad \text{Hz} \quad \text{mm} \quad \text{mm} \quad (2.3)$$

where,

f_n = Natural frequency of ring cps.

R = Spring constant of the ring N/m.

$R = \text{Area of the ring, } R = (\pi r)^2 / 4 \rho t$

In view of the weight of the ring W equation (2.1) reduces to,

$$f_n = \frac{1}{2\pi} \sqrt{\frac{W}{R}} \quad \text{... (2.2)}$$

Spring constant of ring is given by following relation (2.3):

$$R = \frac{1.69 \times h_r \times t^3}{l_0^2} \quad \text{N/m} \quad \text{... (2.3)}$$

2.2 Design Calculations

2.2.1 Material Selection

Requirements of dynamometer ring material are:

- a. good mechanical properties
- b. good machinability
- c. high heat conductivity
- d. light in weight
- e. corrosion resistance

In the present case Alumina was used as the ring material.

2.2.2 Section Sizes of the Rings

The alumina gauge selected as the dynamometer had a gauge factor ($K_g = 4 R / R_0$) of 2.88. These were manufactured by Babbitt & Company (India) Limited.

Four channel recorder manufactured by Recordex Inc. (Paris, U.S.S.R.) was used for recording the forces during grinding. The maximum sensitivity available on this recorder was 50000 volts per mm of deflection.

For four arms active Wheatstone bridge with input voltage of 12 volts equation (3.6) yields,

$$\delta/\delta x = 0.0005 \times 10^{-12} \text{ in/in} \quad \dots \quad (3.7)$$

It was observed that a tensile force of 2 lbs gave 2 mm deflection on the recorder. Therefore, equation (3.6) gives,

$$\delta/\delta x = 0.0005 \times 10^{-12} \text{ in/in} \text{ per } 20 \text{ of force}$$

Assigning the dimensions to obtain various output forces of 200 lbs, we have

$$\delta/\delta x = 200.0 \times 10^{-12} \text{ in/in} \quad \dots \quad (3.7)$$

Dimensions are subjected to repeated testing and validating, therefore at higher strain values the fatigue life of the gauges are considerably reduced. It has been found that a strain gauge has an infinite life when operated at strains below 1000×10^{-12} in/in (0.01%). In the present case maximum strain was much lower than this value.

3.7.2 Maximum Induced Strain

As any instant strain in the ring and the gauges will be the same, the maximum strain (δ_{max}^*) induced in the ring when the maximum normal force is applied is given by

$$\delta_{\text{max}}^* = \delta_{\text{max}} \times 2 \pi \times 1000 \text{ rad.} \quad (0 \text{ for } \Delta l = 10^{-3} \text{ rad.})$$

Third yield stress for aluminum is 2000 MPa which is much higher than the vonmises stress imposed on the ring. Hence ring will not undergo plastic deformation.

3.7.4. Minimum Ring Thickness

For pure shear vonmises stress 0.7938×10^{-3} Taylor strain is given as output of 1.0% on the monitor. If only one axis is active then the output would be changed by $\sqrt{3} = 1.732 \times 10^{-3}$ Taylor strain which is equivalent to

$$\frac{0.7938 \times 10^{-3}}{\sqrt{3}} = 0.46 \times 10^{-3} \text{ strain / m}$$

(where 0.46 denotes the gauge factor)

Assuming unit Φ radius of the ring R_2 to be 1 inch and width of ring equal to $2R_2$ and substituting $\epsilon_0 = 0.46 \times 10^{-3}$ strain/m in equation (3.2) we get

$$R = 4.88 \text{ mm}$$

Re-ordered 4 mm ring thickness. This reduction in ring thickness will increase the sensitivity of the transducer with a slight reduction in its stiffness.

3.7.5. (a) Transducer of Box

The weight of ring was estimated to be 0.81 kg. Equations (3.4) and (3.5) yields

$$f_p = 104 \text{ cps.}$$

Spindle speed of grinding machine was 2700 rpm which gives an excitation frequency of 46 cps.

Thus the calculated frequency of dynamometer ring was more than 0.5 times the cutting frequency which signifies that the measured force will not be influenced by vibrating surface during grinding.

3.3 Resonance Frequency of the Dynamometer

The dynamometer ring was mounted with other components as shown in Fig.(3.2). Due to the various attachments the dynamometer ring was no longer rigid and its natural frequency will be considerably reduced. The exact value was obtained experimentally.

A wave form generator was used to generate sine wave and the signal was fed to a power amplifier. The signal from the power amplifier excited electromagnetic vibration generator which induced vibrations in the dynamometer. The output from the dynamometer was fed to an oscilloscope.

As the frequency of vibration was gradually increased until the natural frequency of the dynamometer was reached. At this frequency the amplitude increased significantly indicating resonance condition. This frequency was 578 cps which was about 3 times more than the cutting frequency.

3.4 Calibration of the Dynamometer

Four weights of the dynamometer were calibrated using dead weights and a pulley system as shown in Fig. (3.3). By plotting the calibration curve, it was found that the dynamometer had linear calibration. Some cross-sensitivity was also observed between the two channels.

Method of least square was used to find the equation of line of best fit through the experimental points. This is summarized below:

$$R_n = K_{nn} P_n + K_{nL} P_L \quad \dots \quad \dots \quad (3.8)$$

$$R_L = K_{Lnn} P_n + K_{LL} P_L \quad \dots \quad \dots \quad (3.9)$$

where,

R_n = Total deflection on the normal force channel

R_L = Total deflection on the tangential force channel

P_n = Normal force

P_L = Tangential force

K_{nn} , K_{nL} , K_{Lnn} and K_{LL} are constants of equilibrium curves.

From which we get,

$$\sum (a R_n)^2 = \sum R_n = K_{nn} P_n + K_{nL} P_L \quad \dots \quad (3.10)$$

The necessary conditions for $\sum (a R_n)^2$ to be minimum are,

$$\frac{\partial (\sum a R_n)^2}{\partial R_n} = \frac{\partial (a R_n)^2}{\partial R_n} = 0 \quad \dots \quad (3.11)$$

Equation (3.11) also coupled with condition (3.10) yields,

$$K_{nn} = \frac{\sum R_n P_n}{\sum P_n^2} \quad \text{con (Normal force)} \quad \dots \quad (3.12)$$

$$\text{and} \quad K_{nL} = \frac{\sum R_n P_L}{\sum P_L^2} \quad \text{con (Tang. force)} \quad \dots \quad (3.13)$$

Initially constants of equation (3.8) were found to be,

$$K_{nn} = \frac{\sum R_n P_n}{\sum P_n^2} \quad \text{con (Normal force)} \quad \dots \quad (3.14)$$

$$T_{\text{SL}} = \frac{\sum_{i=1}^n P_{i,1}}{\sum_{i=1}^n P_{i,2}} \quad \dots \text{for } \text{SL} \text{ case} \quad \dots \quad (2.13)$$

From equations (2.12) to (2.13) we get the following estimation equations:

$$R_0 = 0.1007 P_{1,1} + 0.0034 P_{1,2} \quad \dots \quad (2.14)$$

$$R_1 = 1.3229 P_{1,1} + 0.2330 P_{1,2} \quad \dots \quad (2.15)$$

A program was developed to find R_0 & R_1 from the measured values of Reflections $R_{1,1}$ and $R_{1,2}$:



FIG. 2-1 CIRCULAR FRAME



FIG. 2-2 RECTANGULAR FRAME

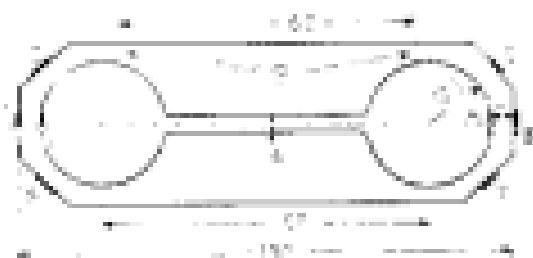


FIG. 2-3 HORIZONTAL BEAM WITH DYNAMIC LOADS

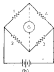
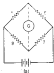


FIG. 2-4a, b. HORIZONTAL DIRECTIONAL FORCE CIRCUIT
DEVELOPED FROM HORIZONTAL DYNAMIC LOADS

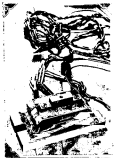


FIG. 2-5. DIPLOPODITES WITH THE
SHELL FRAGILE AND WEAKLY

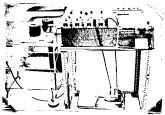


Fig. 26. Construction of the printing press.

CHAPTER 2

EXPERIMENTAL DETAILS

2.1 Grinding Machine

A multi-purpose precision horizontal surface grinding machine manufactured by Koker Precision Tool, Plaza Vytalak, U.S.S.R. was used under pre-planned conditions for the experiments. Some specifications of the machine are given below:

- a. Table dimensions (1000 x 300) mm
- b. Table longitudinal feed speed ranges - 10 mm/min
minimum = 0.5 mm/min
- c. Least count of vertical feed hand wheel: 0.001 mm
- d. Maximum vertical stroke of grinding head: 275 mm
- e. Grinding wheel details: (i) diameter = (100 x 16 x 16) mm
(ii) Spindle rpm = 3750
(iii) Peripheral speed = 30 m/sec

Machine was equipped with standard electro-magnetic plate.

2.2 Balancing of Grinding Wheel

All grinding wheel used were balanced using test weights. Heavy weight was first determined (with the weight removed from the counter and marked). Horizontal line 1-0 (Fig. 2.1) is drawn and weights were inserted

in the count of 45° above and below the horizontal line. The two top weights were slightly moved upward to bring them closer. If out of balance still existed the bottom weights were moved towards the horizontal line. The position of the heavy spot was located, which was 10° away from the former position. This caused to the new position of heavy spot previous procedure was repeated until the wheel did not turn which indicated that the wheel was balanced.

3.2 Grinding Accuracy:

Spunwires are mounted on the spindle base of the table and grinding motion was started. Grinding time of 15 minutes was allowed before performing tests, which were carried out to ensure the following:

(a) Current testing:

First stage of the grinding sheet will appear in a thin circular ring, mounted on it, when the wheel is moving. Absence of such appearance on sheet face ensures the concentricity with respect to the spindle and hence correct testing.

(b) Standardization of the dressing technique:

Different tools were used for dressing and dressing. A new sharp pointed ground diamond was employed for dressing. The dressing diamond was mounted on a tool post with the natural cleavage point vertically upward and was made to touch the sheet at the bottom most point. Free dressing under the following conditions gave repeatable results:

- (i) free passes at cross clearance of 1.0 degree with depth of cut of 0.015 mm.
- (ii) free passes at cross clearance of 1.0 degree with depth of cut of 0.005 mm.

(a) Speed test.

Here one can move front to rear and rear to front ratios of dressing tool at a given depth of cut at the beginning of the dressed action.

(a) Proper positioning of the experimental setup.

The grinding apparatus (discussed in chapter 3) was specially designed and fabricated for the purpose. Self-aligning arms of the dynamometer were purposed to keep the magazine and grinder. Positioning of the dynamometer and the flexibility and consistency of the gauge circuits under continuous grinding. Proper working of the recorder and hydrolic drive of the grinding machine was also verified.

(a) Number of passes required to equilibrate the dressed and the cut.

At the start of the grinding the depth of cut required will be a function of densities due to the elasticity of the system. If the steel is fed forward successively during each cycle the depth of cut will quickly approach the densities. Number of such strokes required was found to vary between 15 and 20. After this equilibrium condition was reached the former were removed.

(a) Methods of establishing the beginning of conjugating points.

The following phenomena were observed when grinding reaches re-dressing point:

(i) Displacement of dressing rod suddenly increased showing sharp increase in grinding forces.

(ii) Workpiece surface had changed to with lesser adhesion resulting in

undulations hence. This was due to high grinding temperature in the region of re-heating point.

- (ii) Flare surface finish was variable.
- (iii) Notches appeared around the weld from indicating improper tooling or weld.
- (iv) Side flaps of the cover along the edges of the welds were observed indicating ploughing and very little cutting.
- (v) Increase in vibration was observed.

3.4 Rotating conditions:

- (i) Workpiece: The dimensions of workpiece are shown in Fig. (3.3). It was made out of solid (30 x 30) mm² mild steel plate.
- (ii) Grinding Wheel: Grinding wheels of three different hardness and grain sizes were used. These wheels were supplied by Dukarunia Universal Ltd., Noida (India). Their details are given below:

 - 1. $d = 30 \times 20 \times 7.16$
 - 2. $d = 30 \times 20 \times 7.16$
 - 3. $d = 30 \times 20 \times 7.16$
 - 4. $d = 30 \times 18 \times 7.16$
 - 5. $d = 30 \times 20 \times 7.16$

- (iii) Table Speeds: 8 rpm/s, 10 rpm/s and 12 rpm/s
- (iv) Depth of Cut: 0.005 mm, 0.010 mm and 0.015 mm
- (v) Wheel Speed: kept constant at 20 rpm

(1) Dry Bedding:

(2) Wet Bedding:

3.3 Procedure of Experiment:

The dynamometer was mounted on magnetic base of the grates and workplace was brought in the centre of the sheet. The table speed was set at the required value and then sheet was started. Fifteen minutes warmup time was allowed for the complete setup. Finally depth of cut was given during each operation and forces were measured. A representative force measured during experiment is shown in Fig. (3.4). After each time (about 100 cycles/min) machine was stopped and vibration in sheet diameter was measured by stick gauge (Error about 0.001 in.). Vibration in workplace height was also measured with the accuracy of 0.02 in. Sheets were continued until the bedrock condition was reached.

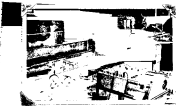
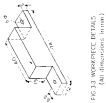


Fig. 11. *Shirakawa no yatai* (Shirakawa Festival Float).



Fig. 2-2. *Dicroidium* (D. *luteum*).



2011-2012 学年第二学期 11 月 11 日至 11 月 25 日

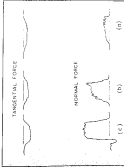


FIG. 14. REPRESENTATIVE PAPER RECORD.

CHAPTER 4

GRINDING FORCES

4.1 Forces Observed

Typical traces of tangential and normal forces are shown in Fig. 4.1(a). It is seen from the traces that the normal force shows more fluctuations than the tangential force. However, variation in the peak value of the normal force is small until about 1/3 of sheet life is reached as shown in Fig. 4.1(a). It appears from these traces that the deformation of the workpiece due to grinding heat is responsible for the variation in normal forces. Thermal deformation of the workpiece increases as the sheet approaches recontacting point, producing increased variation in normal force at grinding process. Normal force trace (Fig. 4.1(a)) just after the sheet life is reached shows that thermal deformation of the workpiece to so high that stable normal repeat process is not possible. The tangential force traces, however, show negligible variation irrespective of grinding time.

4.2 Forces Observed During Stripping

Using the reported values of deflection, normal and tangential forces during grinding were calculated from the utilization equations 2.18 and 2.21. For various grinding conditions, variations of normal and tangential force with number of agglomerates were plotted as shown in Figs. 4.1 to 4.11.

These curves are similar to those obtained by previous workers (30, 31). It is seen from the plots (4.11, 4.12, 4.13, 4.14 and 4.15) that for the same material removal rate higher forces are obtained for the harder steel (lower grain size) as well with bigger grain size (lower hardness). These results are similar to those previously reported (30, 31).

Typical force patterns (4.1) can be divided into three regions in the case stated in the two above discussed machine:

- (i) an unstable region where the force rises to a peak and then falls to a steady value when stable wear that is developed in sharp grains.
- (ii) a region of stable grinding conditions where forces are constant and level in an equilibrium. It means that in this region the effect of trying to push out the worn off and truly equal steel is obtained. However, this region can only obtained at low material removal rate (Fig. 4.1).
- (iii) a region of progressive build up of forces follows the region of stable grinding condition, where attrition wear is predominant. Length of this region depends upon the reaction of the steel to the particular composition of table wear and depth of cut.
- (iv) a region of sharp increase in force when cutting of grain reaches a critical value and overcutting develops, thereby workpiece loses grinding because insufficient and redepositing is required to regain the cutting ability of the grains.

From Fig. (4.15) and Fig. (4.12) exhibits a constant force during grinding (indicating the possibility that stable attrition) and 400-50-200

width of the grinding wheel with material and give predominant fracture wear in regime III.

4.3 Tool Life of Grinding Wheel:

From the normal and tangential force patterns, and of phase II was preferentially selected for both components of grinding force. The data of these two values are taken as the point where phase III begins. This defines the tool life of grinding wheel in terms of the number of operations (N^*), which is converted into seconds by using the following formula :-

$$T^* = \left(\frac{0.001}{\pi} \frac{b_0}{v} \right) N^* \quad \text{...} \quad \text{...} \quad (4.1)$$

where,

T^* = Tool life of grinding wheel, seconds

b_0 = Length of workpiece, mm

v = Table speed $v = v_1 v_2$ m/min

Rate of material removal is estimated by using following formula :-

$$V_R = \frac{v \cdot b_0 \cdot d}{48} \quad \text{...} \quad \text{...} \quad \text{...} \quad (4.2)$$

where,

V_R = Rate of material removal, cm^3/sec

b_0 = Width of workpiece, mm

d = Depth of cut, mm

Table (4.1) shows the wheel life and the material removal rate for some sets of working conditions.

Table (b)

test	Grinding Conditions		Test Rate of Grinding Steel		Rate of Material removed
	F_r (mm)	X_r (mm)	No. of revs. (min ⁻¹)	Throughput (kg)	
A. 30-30-40-10	30	40	200	48.0	0.20
A. 40-30-40-10	40	40	2000	480.0	2.0
"	30	40	200	120.0	0.20
"	30	30	80	48.0	0.20
"	30	30	600	240.0	0.20
"	30	30	300	120.0	0.20
"	30	30	100	30.0	0.20
"	30	30	80	24.0	0.20
A. 40-10-40-10	40	10	200	48.0	0.20

4.4 Grinding Rating

Power ratings for shovels A. 30-30-40-10 and A. 40-10-40-10 do not show the presence of region III, which indicates that these conditions in the grinding test (10) is not valid under some cutting conditions. In order to evaluate grinding performance under conditions of varying hardness and varying grain size, economic aspects of various cutting conditions (i.e. range of grinding rates) was investigated.

Value of rated rate is calculated by using following relation:

$$V_r = \frac{\sum V_r}{n} + \frac{E(V_r)}{n} = V_r \quad \dots \quad \dots \quad (4.8)$$

where,

$$V_0 = \text{Volume of sheet year} , \text{ m}^3$$

$$D_0 = \text{Sheet diameter} , \text{ m}$$

$$\frac{D_0}{2} = \text{Radius to sheet diameter} , \text{ m}$$

$$h_0 = \text{Width of workpiece} , \text{ m}$$

Four curves showing the variation of volume per sheet year and volume of material removed were plotted. These are shown in Fig. 4.26, and are similar to those obtained by previous workers (37, 48, 50). The slope of the linear portion of these four curves (region II) gives (grinding ratio).

Table (4.2) shows values of material removed, volume per sheet year and grinding ratio for various sheets at a constant rate of material removal.

Table (4.2)

Sheet	Average Ratio
A 45-85-410	5.2
A 45-85-310	69.4
A 45-85-210	90.0
A 35-75-410	26.0
A 35-75-310	37.0

4.6 Material Consumption at the Interface

A 45-85-410 sheet is extensively used for grinding mild steel, which was used in the present investigation also. This sheet was used

under different cutting conditions for establishing the tool-life equation of the grinding steel.

Variation of tool-life with material removal rate is shown in Fig. 4.11(b) which shows that the tool-life of grinding steel decreases with increasing metal removal rate. On log-log scale this appears to be a linear (Fig. 4.11(b)). These are limited experimental data and necessary conclusions can be drawn. In the table cited we measured the slope of the line determined and these lines appear to intersect at about one point on the tool-life axis. Since this, however, should be verified from data for various steel grades. However, this appears to be reasonable from the consideration of brittle cutting as an individual process. The linear plot of Fig. 4.11(b) based on these limited results appears to be related to the material removal rate by the following equation:

$$T = (T_0)^2 \cdot e^{-C \cdot v} \quad \dots \dots \dots \quad (4.4)$$

where

T = Tool-life of grinding steel; T_0 = Intercept removal rate

C = Slope constant which depends on the steel used

v = Table speed

e = Slope constant, which depends on the grinding steel indicated with the consideration of optimum grinding performance for the given material.

4.2 Linear Extrusion Analysis of the Process

4.2.1 Decomposition of Tool-life Relations

Method of linear square can used to obtain the type of tool-life between the variables $\log T^2$ and $\log T_0$.

Equation (4.4) can be written as

$$\log \Omega^2 = \log C + a \log N_{\text{H}} \quad \dots \quad (4.5)$$

Assuming that the equation (4.5) represents line of best fit through the experimental points $(\log N_{\text{H}1}, \log \Omega_1^2)$, $(\log N_{\text{H}2}, \log \Omega_2^2)$, ..., $(\log N_{\text{H}n}, \log \Omega_n^2)$, the sum of the errors of the distances of experimental points from line (4.5) is given by,

$$\eta = \sum_{i=1}^n \left[(\log \Omega_i^2 - \log C + a \log N_{\text{H}i}) \right]^2 \quad (4.6)$$

Minimization of $\log \Omega$ from equation (4.6) using equation (4.5) yields,

$$\eta = \sum_{i=1}^n \left[(\log \Omega_i^2 - \log \Omega^2) + a (\log N_{\text{H}i} - \log N_{\text{H}}) \right]^2 \quad (4.7)$$

η decreases when a , and Ω , is chosen such that η is minimum. The necessary condition for this is,

$$\frac{\partial \eta}{\partial a} = 0 \quad \dots \quad \dots \quad \dots \quad (4.8)$$

Equation (4.8) when operated with condition (4.5) yields

$$a = \frac{\sum (\log \Omega_i^2 - \log \Omega^2) (\log N_{\text{H}i} - \log N_{\text{H}})}{\sum (\log N_{\text{H}i} - \log N_{\text{H}})^2} \quad (4.9)$$

In the above equation $\log \Omega^2$ and $\log N_{\text{H}}$ represents mean value of the variables satisfying the line of best fit in equation (4.5). The value of dynamic constant calculated from equation (4.9) can be used in equation (4.4) for calculating the static constant.

Table 4.4(i) shows calculated values of the constant α and table speed.

Table 4.4(i)

N_r cycles	Dynamic constant, α^2	Dynamic constant, α^2 calculated, α
8	2.304	2.304
12	1.897	1.897

4.4.2 Effect of dynamic constant

The general form of best-fit equation for 2.4823-PIE model is,

$$2\pi N_r T^2 = 2.4823 \quad \dots \quad (4.10)$$

Using the experimental values for N_r and T^2 , $T^2 = 20.0$ and $N_r = 6.2$ $\text{deg}^2/\text{min}^2$ at static stress of 10 cycles, equation (4.10) yields

$$\alpha = 1.782$$

It is seen from these results that dynamic constant decreases with increase in table speed. On log α vs log T^2 plot, Fig. (4.10) variation of dynamic constant with table speed appears to be linear, which reveals that the dynamic constant must be related to the table speed by the following equation:

$$\log \alpha = a + \log T^2 + \log E_0 \quad \dots \quad (4.11)$$

$$48 \quad \alpha = e^a \cdot T^2 \cdot E_0 \quad \dots \quad (4.12)$$

Assuming that equation (4.11) represents the best-fit, the stress $\sigma = \sigma_0 \cdot T^2$ is given by the following equation deduced from equation (4.6)

$$\frac{\sum (\log n_i - \log \bar{n}) (\log r_i - \log \bar{r})}{\sum (\log r_i - \log \bar{r})^2} \quad (4.12)$$

From equations (4.11) and (4.12) n and K are found to be 2,029 and 3,094 respectively.

Thus equation (4.11) becomes,

$$n = (2,029) (r)^{-0.298} \quad \dots \quad (4.13)$$

Substitution for n in equation (4.10), gives us the final equation for the grinding wheel life,

$$T = (r)^{0.398} (v)^{-0.298} \quad \dots \quad (4.14)$$

This equation is very similar to Taylor's tool-life equation and can be used to express the tool-life of grinding wheel.

Material removal rate in grinding is proportional to the product of table speed and depth of cut. Hence, tool-life equation (4.14) shows that increase in depth of cut sharply affects the tool-life. Therefore for the same material removal rate, table speed should be fixed as high as possible depending on surface finish requirements and then depth of cut should be adjusted accordingly. With the present work it is recommended that for increasing the material removal rate, the table speed should be increased not not the depth of cut.

4.7 Prediction of Theoretical Values of Tool Life

Theoretical values of tool-life for a 46-50-700 wheel which were established from four patients (Figs. 4.1, 4.2, 4.3, 4.5, 4.7) were

compare with the theoretical values predicted by tool-life equation (4.15). These are given in table (4.4).

Table (4.4)

v m/min	$\frac{v_g}{v}$ mm/min	T_g Theoretical (Experimental)	
		min	min
5	0.0	100	100.0
5	2.0	175.0	175.0
5	4.0	250.0	250.0
10	4.0	150.0	150.0
10	6.0	21.0	20.0
10	10.0	11.0	10.0
15	6.0	9.0	9.0

The tool-life equation (4.15) which was established from the experimental results, reproduces the tool-life values with very little difference. This indicates that equation (4.15) can be used to predict accurately the tool-life for A-60-20-210 wheel under different cutting conditions.

4.8 Selection of Grinding Wheel

The important parameters in the selection of grinding wheel are grade (diamond) and grain size. Previous results (37) used to suggest that there are optimum values of grade and grain size of grinding wheel for a particular work material for economic machining. The tool-life

equation (4.11) should be used only after a suitable sheet has been obtained. In order to investigate the opposite aspect of grinding with different steels, grinding ratios were plotted (Figs. 4.20 and 4.21) against steel hardness and grain size. Fig. 4.20 shows the variation of grinding ratio with steel hardness. This indicates that as the steel hardness is increased, grinding ratio decreases and reaches an optimum value for J hardness, while further increase in steel hardness lowers the grinding ratio. Similar variation in grinding ratio is observed when grain size is increased from 30 to 40 with the optimum value of grinding ratio occurring for 40 grain size (Fig. 4.21). These results agree with those obtained by previous authors (Fig. 12).

The steel with hardness H being a soft steel is likely to have high resistance over to interaction with abrasive wear. As the sheet hardness increases, for the same grain size, the amount of friction will still decrease and interactions over will increase. At low hardness the high compressive between interactions and fracture over is likely to reach where an optimum grinding ratio will be obtained. This signifies good grinding conditions. As the hardness of the sheet is increased from J to L interactions over increases significantly. Grinding force, being strongly dependent on the over flat area, will also increase. This increases the probability of grain fracture. Thus harder steel is likely to have high interactions over and significant grain fracture along with decreased material removal rate. This is also seen in Fig. 4.21 which indicates that A 40-40-400 sheet

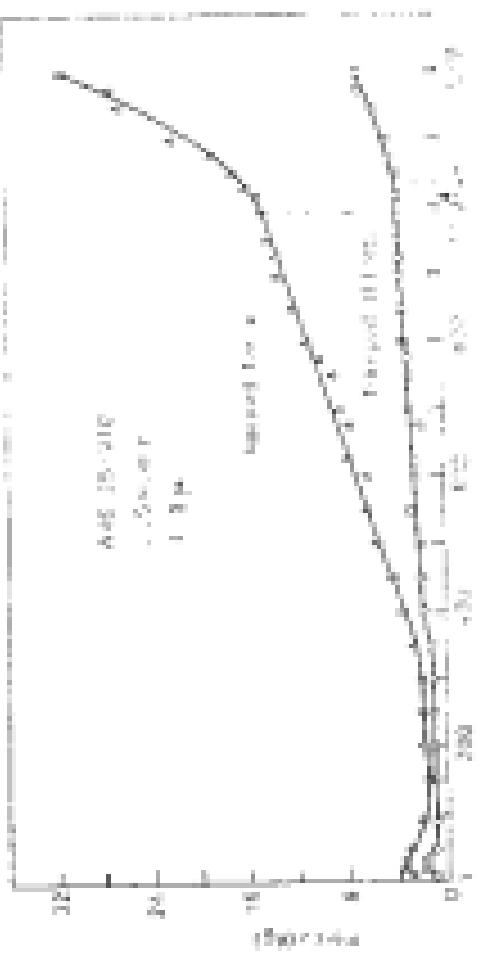
have higher wear rate than that of 200-400 but lower than that of 4-500-500.

The reverse phenomena is likely to occur when grain size is increased from 20 to 40 (increasing grain size under same smaller grain diameter). This is shown in Fig. (1.11). For media with larger grains, say 30, large retaining zones will be generated giving high attritioning wear and subsequently high grinding forces, which is likely to cause more grain fracture. For smaller grains (high grain size number), friction wear is likely to dominate attrition wear. In between these two extreme phenomena the optimum grinding media is likely to be obtained. It may be pointed out that the selection of grain size of a steel is also based on the surface finish requirements. Higher grain size number gives better finish (28, 43).

Variation of volume of material removed for different steel hardness and grain sizes in grinding process are shown in Fig. (1.12). It is seen from the plot that the maximum material removal for 4-100-400-400 steel and minimum for 4-300-300 steel weight losses for steel, with differences like between the two and hence dropping characteristics in grinding process. This is due to the fact that harder steels have more loading with odds, thus reducing the volume of material removed. Similar curves for media with different grain sizes but same hardness are shown in Fig. (1.13). The figure indicates that 40 grain size steel will remove maximum volume of material and 30 grain size steel will give least material removal (due to steel loading), while curve for 60 grain size steel lies between the two and hence dropping characteristics in grinding process.

It appears from the above discussion that if the steel grain is in the self sharpening or predominant leading rough grinding ratio will be 100. However, in between these two, in certain grinding conditions certain steel points in a time of mixed conditions - partly self sharpening and partly leading, giving certain grinding ratios.

FIG. 2.1. PULSE-PULSE PATTERN, LINEAR, 1000



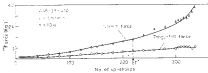
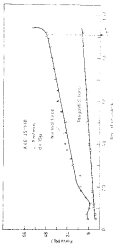


FIG. 4.2 FORCE PATTERN DURING DRIVING.

FIG. 4.3. ESR spectra of Fe^{2+} in Fe_2O_3 at 77°K (a) and 15°K (b).



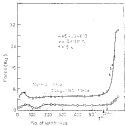


FIG. 4-4 FORCE PATTERN DURING SWINGING

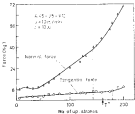


FIG. 4-5 FORCE PATTERN DURING SWINGING

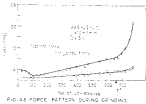


FIG.4.3 FORCE PATTERN DURING GRINDING.

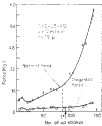


FIG.4.4 FORCE PATTERN DURING DRILLING.

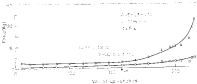
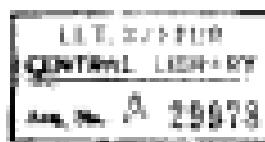
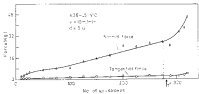


FIG. 4.8 FORCE PATTERN DURING LANDING.





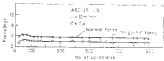


FIG. 4.10. FORCE VARIATION DURING QUENCHING.

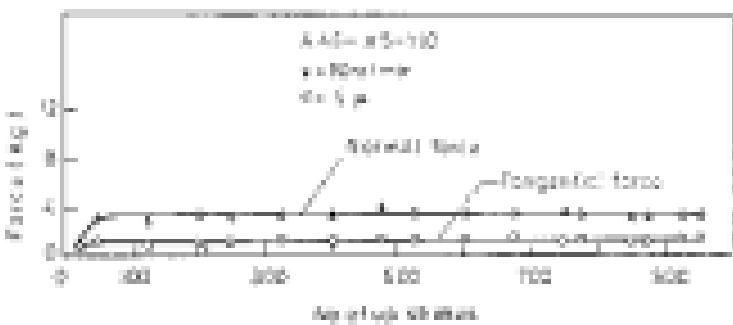
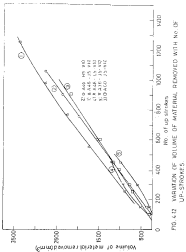
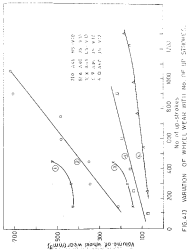
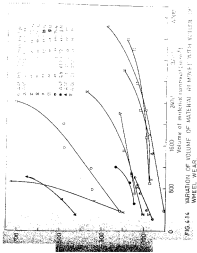


FIG. 4.11. FORCE VARIATION DURING QUENCHING.







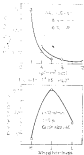


Fig. 3. (a) Location of point 'a' in the 400C residue

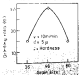


Fig. 4. (b) Location of point 'b' in the 400C residue

Fig. 4. A. Effect of T_{max} on P_{max} (1000 rpm).

Box of bottles measured
(1000 rpm)



Fig. 4. B. Effect of T_{max} on P_{max} (1000 rpm).

Box of bottles measured
(1000 rpm)



Fig. 4. C. Effect of T_{max} on P_{max} (1000 rpm).

Box of bottles measured
(1000 rpm)



3.3 Revised Dressing of the Tool-Work

Present work may provide a guideline for levelling the point during grinding when sheet material dressing. Thus, approach when grinding due to uncertainty in sheet dressing may be refined.

3.4 Opportunities

By performing the trials during wet grinding under a wide variety of working conditions, the tool-life criterion established in the present work may be translated into an ideal and practical form. Moreover, tool-life may also be investigated with the considerations of sheet size and performance.

REFERENCES

1. R.W. Hartmann, "An anisotropic ice Cracking Process", *Adv. in Ceram.*, Vol. 42, March 1987, p. 45.
2. J.M. Dugue, "Cylindrical fracturing in ICP", *Trans. AICM*, vol. 40, 1988, p. 293.
3. G.J. White, "Operation of fracturing cracks in Nuclear Reacting", *Trans. AICM*, vol. 40, 1988, p. 301.
4. R.J. Dugue, "The Concepts of Stressors: Prediction of Fracture Cracking Performance", *Int. J. Fract.*, Vol. 14, 1978, p. 225.
5. L.P. Parker, "Fracture Performance of Concrete", *Int. J. Fract.*, Vol. 14, 1978, p. 135.
6. S. Suresh, "A study of debonding paths by single劈裂", *Journal of the CIBF*, vol. 13, 1986, p. 185.
7. G.M. Friedman, R.L. Tsai & P.J. Burchett, "Interpretation of Stress-Strain Properties of Cyclic Debonding Paths", *Trans. AICM*, p. 295, July 1973.
8. S. Suresh, C. Dowling & C. Turner, "Fracture and Debonding in Cyclic Loading with regard to the Debonding process", *Proc. Int. Debonding Seminar*, Carnegie-Mellon University, Pittsburgh, USA, April, 1973, p. 359.
9. S. Suresh, "The Debonding of Concrete", *Proc. Symp. on Tech. of Cyclic Debonding*, L. Neth. R. C. Berlin, 1988.
10. J.M. Dugue, "A Review of Debonding of Metal Inclusions in Cracking", *J. Mech. Phys. Solids*, vol. 31, No. 3, 1983.
11. G.J. White & R.J. Dugue, "On the Debonding of Debonding Debonds", *Int. J. Fract.*, vol. 13, No. 3, Sept. 1973, p. 331.

35. R.L. Edm., "On the nature of Grinding Resonance", Proc. Inst. Mech. Eng. Vol. 196, Part 2, 1962, p. 229.

36. T. Suzuki and K. Ogawa, "The cutting mechanism of abrasive grain", Bull. Japan. Soc. of Mech. Engg., Vol. 3, 1960, p. 661.

37. W.R. Cook, R.J. Lowe & R.A. Shaw, "Abrasive Tool Breakdown - a Current Appraisal", Research Institute, Eng. 10, 1964, vol. 10, p. 128.

38. R.S. Jones, R.S. Marshall & G.J. Shaw, "Electric Discharge Tool Breakdown", Presented at the Society's Spring Meeting in Cleveland Ohio, May 27, 1962.

39. G.J. Shaw, "Design of Surface Grinding Spindle", Trans. ASME, J. Engg. Ind., Feb. 1958, p. 157.

40. G.J. Shaw & R. Barker, "On the Use of Grinding Wheel", Proc. (in press).

41. G.J. Shaw & R.A. Shaw, "Use of single abrasive grain in fine grinding", Proc. Inst. Grinding Inst., Cleveleyton Hall, Pittsburgh, PA, April 18-19, 1970, p. 101.

42. G.J. Shaw, "Design in Practical Surface Grinding", Inst. J. Mach. Tools Mater., vol. 8, 1968, p. 35.

43. G. McHugh & R.J. Cook, "The Use of Grinding Tools Part 2: Materials", Trans. ASME, J. Engg. Ind., vol. 83 B, Nov. 1961, p. 1128.

44. G. McHugh & R.J. Cook, "The Use of Grinding Tools Part 3 - Structure Tools", Trans. ASME, J. Engg. Ind., vol. 83 B, Nov. 1961, p. 1139.

45. R.J. Barker & R.J. Krishnamo, "New Techniques in Metal Cutting Research", Trans. ASME, vol. 78-8, 1956, p. 243.

46. G.J. Shaw & R.J. Williams, "The Use of abrasives in Grinding", Mach. Engg., vol. 83, p. 1, 1961, p. 48.

47. R.J. Krishnamo, "Factors Affecting the Use of Grinding Wheels", Trans. ASME, J. Engg. Ind., Vol. 81 B, Aug. 1959, p. 107.

36. T.J. Wetherholt, "Wheel Wear and Surface Finish in Crossfeed Surface Grinding", Int. J. Mach. Tool Des. Res., vol. 20, No. 2, Sept., 1980, p. 285.

37. H. Yoshikawa & T. Sato, "Study on Wear of Grinding Wheel in Feed Traversing in Grinding Thread", Trans. ASME, J. Engg. Ind., vol. 80 (8), 1958, p. 384.

38. P. Petters, "The Wheel Wear and Metal Removal Mechanism in Vertical Spindle Threading of Thread", Trans. ASME, 1957.

39. R.P. Disney & R.J. Baker, "On the Basic Relationship between Grinding Parameters", Annals of the C.I.M.F., 1973, p. 387.

40. P.J. Bissinger & M.J. Miller, "Wheel Wear Patterns in Surface Grinding", Manufacturing Research, Feb. 1980, p. 38.

41. J. Kannappan & R. S. Sankar, "Effect of Wheel Size and Operating Parameters on the Mechanics of Grinding", Trans. ASME, J. Engg. Ind., 1970.

42. H. Yoshikawa, "Relation: Wear of Grinding Thread", Proc. Int. Conf. Prod. Engg. Inst., 1960, vol. II, No. 2, p. 316.

43. H. Yoshikawa, "Thread Grinding Research", Production Engineer, May-June 1960, p. 59.

44. H. Yoshikawa, R.J. Miller & P.J. Varley, "Selected Factors of Grinding Process: Wheel Wear and Surface Finish", Int. Prod. Res., vol. 10, No. 4, Sept., 1972, p. 317.

45. D.R. Marshall & C.J. Shaw, "Process in Dry Surface Grinding", Trans. ASME, vol. No. 1952, p. 34.

46. D.R. Disney, "Wear and Form Relation in Grinding with Coated Abrasives", Trans. ASME, J. Engg. Ind., vol. 80 (8), 1958, p. 387.

47. P.J. Bissinger & M.J. Miller, "Process in Surface Grinding with Internally Coated Tools", Manufacturing Research, Feb. 1980, p. 38.

48. M.C. Shaw & C.J. Shaw, "An Analysis of Surface Grinding of Glass Surface", Trans., 1952, J. Engg. Ind., 1952, p. 345.

Mr. R.P. Bhowmik, B.I.E., D.Sc., "Variables Affecting Steel Strength and Strength Loss in Precipitation Hardening", *Annals of IDP*, vol. 10/1, 1971, p. 41.

Mr. G.D. Gurley, "Evaluating the Performance of Retarding Agents", *Resinous Bags*, August 1981, p. 38.

Mr. R. Golding, "Application of the Retarding Approach", *Annals IDP*, vol. 10/1, 1971, p. 42.

Mr. R. Golding, "Theory of Steel Alite for the Retarding Agent", *Annals IDP*, vol. 14, 1975, p. 443.

Mr. G.D. Gurley & Mr. Golding, "Predicting Steel Alite of Retarded Hardening", *Resinous Bags & Management*, Vol. 15, No. 1, May 1981, p. 31.

Mr. G.D. Gurley, "Prediction of Strength Loss in Hardening", *Trans. IDP*, 1980, 1, Aug. 1980, p. 446.

Mr. R.P. Bhowmik, "The Effect of Retarding Substances in Precipitation Hardening", *Trans. IDP*, 1980, 1, Aug. 1980, p. 449.

Mr. Golding, J. Gardner & R.C. Rose, "Retarding Steel Hardening", *Trans. IDP*, 1980, 1, Aug. 1980, p. 459.

A29878

MG-132 + H = MG H + SfU

A29578

MEETINGS-MEETINGS